Applied Mathematics, 2013, 4, 18-28
http://dx.doi.org/10.4236/am.2013.45A003 Published Online May 2013 (http://www.scirp.org/journal/am)

High-Order Spectral Stochastic Finite Element Analysis of Stochastic Elliptical Partial Differential Equations

Guang Yih Sheu[1,2]
[1]Department of Accounting and Information System, Chang-Jung Christian University, Gueiren, Tainan, Taiwan
[2]Department of Civil Engineering, Feng-Chia University, Taichung, Taiwan
Email: xsheu@hotmail.com

Received February 27, 2013; revised April 23, 2013; accepted April 30, 2013

ABSTRACT

This study presents an experiment of improving the performance of spectral stochastic finite element method using high-order elements. This experiment is implemented through a two-dimensional spectral stochastic finite element formulation of an elliptic partial differential equation having stochastic coefficients. Deriving this spectral stochastic finite element formulation couples a two-dimensional deterministic finite element formulation of an elliptic partial differential equation with generalized polynomial chaos expansions of stochastic coefficients. Further inspection of the performance of resulting spectral stochastic finite element formulation with adopting linear and quadratic (9-node or 8-node) quadrilateral elements finds that more accurate standard deviations of unknowns are surprisingly predicted using quadratic quadrilateral elements, especially under high autocorrelation function values of stochastic coefficients. In addition, creating spectral stochastic finite element results using quadratic quadrilateral elements is not unacceptably time-consuming. Therefore, this study concludes that adopting high-order elements can be a lower-cost method to improve the performance of spectral stochastic finite element method.

Keywords: Spectral Stochastic Finite Element Method; Generalized Polynomial Chaos Expansion; High-Order Elements

1. Introduction

A stochastic partial differential equation is a partial differential equation having stochastic coefficients or forcing terms. Problems expressed as stochastic partial differential equations include such as population dynamics and elastostatics with the uncertainty in the spatial variability of mechanical properties. The spectral stochastic finite element method [1] may be the most popular numerical tools for solving stochastic partial differential equation. Briefly, deriving a spectral stochastic finite element formulation couples a deterministic finite element formulation and representations of those stochastic coefficients and forcing terms. These representations of stochastic forcing terms and coefficients are derived by such as generalized polynomial chaos [2] and Karhunen-Loève expansions [3].

Numerous spectral stochastic finite element formulations are available for some branches of science and engineering. References [4,5] are two recent examples. Nevertheless, the performance of spectral stochastic finite element method is not always satisfactory. For example, the spectral stochastic finite element method predicts less accurate mean values or standard deviations of random fields than the spectral stochastic meshless local Petrov-Galerkin method does [6]. Similar experiences bring about the motive for improving the performance of spectral stochastic finite element method.

Since a spectral stochastic finite element formulation contains a deterministic finite element solution and random field representations, improving the performance of spectral stochastic finite element method may be through adopting more accurate deterministic finite element formulation or random field representations. Available studies (e.g. [1]), which were devoted to evaluate the performance of spectral stochastic finite element method, seem to focus on the latter method. Experiences of applying a spectral stochastic finite element formulation using high-order elements seem to be unavailable. After a web search, only Ngah and Young (2007) [7] had adopted quadratic quadrilateral elements to predict the

performance of composite structures. Thus, this study focuses on applying the spectral stochastic finite element method using high-order elements and evaluating the accuracy of corresponding spectral stochastic finite element results. A two-dimensional elliptical partial differential equation having stochastic coefficients is chosen as the model problem. A spectral stochastic finite element formulation of such a stochastic partial differential equation is derived by coupling a two-dimensional deterministic finite element formulation of an elliptical partial differential equation with generalized polynomial chaos expansions of stochastic coefficients. Two benchmark problems having deterministic analytical solutions are then introduced to test the performance of resulting spectral stochastic finite element formulation with adopting linear and high-order finite elements.

The remainder of this study is organized in three sections. Section 2 presents the two-dimensional spectral stochastic finite element formulation of an elliptical partial differential equation having stochastic coefficients. Section 3 evaluates the performance of resulting spectral stochastic finite element formulation. Based on this performance evaluation, Section 4 draws some conclusion.

2. Spectral Stochastic Finite Element Formulation

Suppose x and y are the spatial coordinates, θ is an event in the probability space, Ω is a problem domain, and Γ is its boundary. The model problem of this study is described by

$$-\frac{\partial}{\partial x}\left(a_{11}\frac{\partial u}{\partial x}+a_{12}\frac{\partial u}{\partial y}\right)-\frac{\partial}{\partial y}\left(a_{21}\frac{\partial u}{\partial x}+a_{22}\frac{\partial u}{\partial y}\right)+a_{00}u-f=0 \tag{1}$$

where u is the unknown (such as temperature and stream function), $a_{ij}\left(i,j=1 \text{ to } 2\right)$, a_{00} and f are coefficients. In addition, the unknown u, coefficients a_{ij}, a_{00}, and f are dependent upon x, y, and θ. Meanwhile, boundary conditions are

$$u=U_0 \text{ on } \Gamma_U \tag{2a}$$

$$q_n=n_x\left(a_{11}\frac{\partial u}{\partial x}+a_{12}\frac{\partial u}{\partial y}\right)+n_y\left(a_{21}\frac{\partial u}{\partial x}+a_{22}\frac{\partial u}{\partial y}\right)=Q_n \text{ on } \Gamma_T \tag{2b}$$

in which U_0 and Q_n are two known functions, Γ_U is the essential boundary, Γ_T is the natural boundary, q_n is the secondary variable, n_x and n_y are the components of a unit vector n normal to Γ_T, and $\Gamma=\Gamma_U\bigcup\Gamma_T$.

To derive a spectral stochastic finite element formulation of (1), a two-dimensional deterministic finite element formulation of an elliptical partial differential equation is needed. Suppose w is the test function. The weak form of (1) is

$$\int_{\Omega^e}-\left[\frac{\partial}{\partial x}\left(a_{11}\frac{\partial u}{\partial x}+a_{12}\frac{\partial u}{\partial y}\right)-\frac{\partial}{\partial y}\left(a_{21}\frac{\partial u}{\partial x}+a_{22}\frac{\partial u}{\partial y}\right)+a_{00}u\right]w\mathrm{d}x\mathrm{d}y=f \tag{3}$$

where the superscript e denotes an element. Simplifying (3) by the divergence theorem yields

$$\int_{\Omega^e}\left[\frac{\partial w}{\partial x}\left(a_{11}\frac{\partial u}{\partial x}+a_{12}\frac{\partial u}{\partial y}\right)+\frac{\partial w}{\partial y}\left(a_{21}\frac{\partial u}{\partial x}+a_{22}\frac{\partial u}{\partial y}\right)+w\left(a_{00}u-f\right)\right]\mathrm{d}x\mathrm{d}y-\oint_{\Gamma^e}wq_n\mathrm{d}s=0 \tag{4}$$

where Γ^e is the boundary of Ω^e, and ds is the arc length of an infinitesimal line along the boundary Γ^e. Next, approximate u over each Ω^e by

$$u\approx\sum_{j=1}^{N}u_j^e\psi_j^e \tag{5}$$

in which N is the total number of nodes in each Ω^e, and ψ is the shape function. Substituting (5) into (4) and setting $w=\psi_i\left(i=1 \text{ to } N\right)$ yield

$$\sum_{j=1}^{N}\left\{\int_{\Omega^e}\left[\frac{\partial\psi_i}{\partial x}\left(a_{11}\frac{\partial\psi_j}{\partial x}+a_{12}\frac{\partial\psi_j}{\partial y}\right)+\frac{\partial\psi_i}{\partial y}\left(a_{21}\frac{\partial\psi_j}{\partial x}+a_{22}\frac{\partial\psi_j}{\partial y}\right)+a_{00}\psi_i\psi_j\right]\mathrm{d}x\mathrm{d}y\right\}u_j-\int_{\Omega^e}\psi_i f\mathrm{d}\Omega-\oint_{\Gamma^e}\psi_i q_n\mathrm{d}\Gamma=0\left(i=1 \text{ to } N\right) \tag{6}$$

Equation (6) can be summarized in the form as

$$\sum_{j=1}^{N}K_{ij}^e u_j^e=F_i^e+Q_i^e \tag{7}$$

where

$$K_{ij}^{e}=\int_{\Omega^e}\left[\frac{\partial\psi_i}{\partial x}\left(a_{11}\frac{\partial\psi_j}{\partial x}+a_{12}\frac{\partial\psi_j}{\partial y}\right)+\frac{\partial\psi_i}{\partial y}\left(a_{21}\frac{\partial\psi_j}{\partial x}+a_{22}\frac{\partial\psi_j}{\partial y}\right)+a_{00}\psi_i\psi_j\right]\mathrm{d}x\mathrm{d}y \tag{8a}$$

$$F_i^e=\int_{\Omega^e}\psi_i^e f\mathrm{d}\Omega \quad\text{and}\quad Q_i^e=\oint_{\Gamma^e}\psi_i^e q_n\mathrm{d}\Gamma \tag{8b}$$

Moreover, (7) can be written more succinctly in matrix algebra as

$$\boldsymbol{K}^e\boldsymbol{u}^e=\boldsymbol{F}^e+\boldsymbol{Q}^e \tag{9}$$

in which $\boldsymbol{u}^e=\left[u_1,u_2,\cdots,u_N\right]$ contain all the nodal u value in each Ω^e. Repeatedly deriving (9) for all Ω^e and assembling all the resulting expressions based on a global numbering system yield

$$\boldsymbol{K}_{(N_T\times N_T)}\boldsymbol{u}_{(N_T\times 1)}=\boldsymbol{F}_{(N_T\times 1)}+\boldsymbol{Q}_{(N_T\times 1)} \tag{10}$$

in which N_T is the total number of nodes in the problem domain Ω. Since $u,a_{ij}\left(i,j=1\text{ to }2\right),a_{00}$ and f are dependent upon x, y, and θ, (10) is not ready for use. The generalized polynomial chaos expansion is chosen to estimate the distribution of $u,a_{ij}\left(i,j=1\text{ to }2\right),a_{00}$ and f. Similar manipulating the published study [6], generalized polynomial chaos expansions of $a_{ij}\left(i,j=1\text{ to }2\right),a_{00}$ and f are defined by

$$\begin{aligned}a_{ij}&=\sum_{I=0}^{N_{PC}}\hat{a}_{ij,I}\left(x,y\right)\Psi_I\left(\boldsymbol{\xi}\right)\\ a_{00}&=\sum_{I=0}^{N_{PC}}\hat{a}_{00,I}\left(x,y\right)\Psi_I\left(\boldsymbol{\xi}\right)\\ f&=\sum_{I=0}^{N_{PC}}\hat{f}_I\left(x,y\right)\Psi_I\left(\boldsymbol{\xi}\right)\end{aligned} \tag{11}$$

where $\boldsymbol{\xi}=\left(\xi_{i_1},\xi_{i_2},\cdots,\xi_{i_{N_{PC}}}\right)$, Ψ_I represent the multivariate orthogonal polynomial of $\boldsymbol{\xi}$, $\xi_{i_1},\xi_{i_2},\cdots$ and $\xi_{i_{N_{PC}}}$ denote multi-dimensional uncorrelated random variables having zero mean and unit variance (for facilitating the computation of mean values and standard deviations of a_{ij},a_{00} and f), N_{PC} is equal to $(n+P)!/n!P!-1$, P is the highest order of Ψ, and n is the total number of uncorrelated random variables.

For facilitating the computation of (11), Ψ_0, $\hat{a}_{i0}\left(i,j=1\text{ to }2\right)$, $\hat{a}_{00,0}$, and $\hat{f}_0$ are; respectively, set to 1, mean values of a_{ij}, a_{00} and f; respectively. Furthermore, computing coefficients $\hat{a}_{ij,I},\hat{a}_{00,I}$, and $\hat{f}_I\left(I=1\text{ to }N_{PC}\right)$ needs the orthogonal relationship,

$$\left\langle\Psi_I,\Psi_J\right\rangle=\left\langle\Psi_I^2\right\rangle\delta_{IJ}\left(I,J=0\text{ to }N_{PC}\right)$$

in which $\left\langle\cdot\middle|\cdot\right\rangle$ is the ensemble average. For example, $\hat{a}_{00,I}\left(I=0\text{ to }N_{PC}\right)$ are computed by

$$\hat{a}_{00,I}=\frac{\left\langle a_{00}\Psi_I\right\rangle}{\left\langle\Psi_I^2\right\rangle} \tag{12}$$

in which $\left\langle\cdot\middle|\cdot\right\rangle$ is computed as follows: If f and g are two functions, $\left\langle\cdot\middle|\cdot\right\rangle$ is computed by

1) Continuous case:

$$\begin{aligned}&\left\langle f\left(\boldsymbol{\xi}\right),g\left(\boldsymbol{\xi}\right)\right\rangle\\ &=\int\cdots\int f\left(\boldsymbol{\xi}\right)g\left(\boldsymbol{\xi}\right)W\left(\xi_{i_1}\right)\cdots W\left(\xi_{i_n}\right)\mathrm{d}\xi_{i_1}\cdots\mathrm{d}\xi_{i_n}\end{aligned} \tag{13a}$$

2) Discrete case:

$$\begin{aligned}&\left\langle f\left(\boldsymbol{\xi}\right),g\left(\boldsymbol{\xi}\right)\right\rangle\\ &=\sum_{\xi_{i_1}}\sum_{\xi_{i_2}}\cdots\sum_{\xi_{i_n}}f\left(\boldsymbol{\xi}\right)g\left(\boldsymbol{\xi}\right)W\left(\xi_{i_2}\right)\cdots W\left(\xi_{i_n}\right)\end{aligned} \tag{13b}$$

where $W\left(\xi_{i_1}\right)\cdots W\left(\xi_{i_n}\right)$ are the weighting functions. In (1), the succeeding study focuses on the continuous random fields; therefore, **Table 1** [6] lists examples of orthogonal polynomials, statistical distributions and weighting functions to generate $\Psi_i\left(i=0\text{ to }\infty\right),\xi_{i_1}\cdots\xi_{i_n}$, and $W\left(\xi_{i_1}\right)\cdots W\left(\xi_{i_n}\right)$; respectively.

Substituting (11) into (8a) yields

$$\begin{aligned}K_{ij}^{e}=&\sum_{I=0}^{N_{PC}}\left(\int_{\Omega^e}\frac{\partial\psi_i}{\partial x}\frac{\partial\psi_j}{\partial x}\mathrm{d}x\mathrm{d}y\right)\hat{a}_{11,I}\Psi_I\\ &+\sum_{I=0}^{N_{PC}}\left(\int_{\Omega^e}\frac{\partial\psi_i}{\partial x}\frac{\partial\psi_j}{\partial y}\mathrm{d}x\mathrm{d}y\right)\hat{a}_{12,I}\Psi_I\\ &+\sum_{I=0}^{N_{PC}}\left(\int_{\Omega^e}\frac{\partial\psi_i}{\partial y}\frac{\partial\psi_j}{\partial x}\mathrm{d}x\mathrm{d}y\right)\hat{a}_{21,I}\Psi_L\\ &+\sum_{I=0}^{N_{PC}}\left(\int_{\Omega^e}\frac{\partial\psi_i}{\partial y}\frac{\partial\psi_j}{\partial y}\mathrm{d}x\mathrm{d}y\right)\hat{a}_{22,I}\Psi_I\\ &+\sum_{I=0}^{N_{PC}}\left(\int_{\Omega^e}\psi_i\psi_j\mathrm{d}x\mathrm{d}y\right)\hat{a}_{00,I}\Psi_I\end{aligned} \tag{14}$$

Table 1. Examples of polynomials and corresponding weighting functions and statistical distributions for generating the generalized polynomial chaos [6].

Distribution	Polynomial	$W(\boldsymbol{\xi})$	Interval
Gaussian	Hermite $H_n(x)$	$\exp\left(-\xi^2\right)$	$(-\infty,\infty)$
gamma	Laguerre $L_n(x)$	$\exp(-\xi)$	$[0,\infty]$
beta	Jacobi $G_n(p,q,x)$	$(1-\xi)^{p-q}\xi^{q-1}$	$[a,b]$
uniform	Legendre $P_n(x)$	1	$[a,b]$

Note that [a, b] denotes a specific interval.

Similarly, substituting (11) into (8b) yields

$$F_i^e = \sum_{I=0}^{N_{PC}} \left(\int_{\Omega^e} \psi_i^e \mathrm{d}\Omega \right) \hat{f}_I \Psi_I \tag{15}$$

Meanwhile, the generalized polynomial chaos expansion of u is

$$u = \sum_{J=0}^{N_{PC}} \hat{u}_J \Psi_J \left(\boldsymbol{\xi} \right) \tag{16}$$

Modifying (10) with (14) and (16) results in

$$\sum_{L=0}^{N_{PC}} \sum_{J=0}^{N_{PC}} \hat{\boldsymbol{K}}_L \hat{\boldsymbol{u}}_J \Psi_L \Psi_J = \sum_{L=0}^{N_{PC}} \left(\hat{\boldsymbol{F}}_L + \hat{\boldsymbol{Q}}_L \right) \Psi_L \tag{17}$$

Requiring the residual resulting from a finite representation of u (*i.e.* truncating $\hat{u}_J \Psi_J, J = N_{PC+1} \cdots \infty$) to be orthogonal to the approximation space spanned by Ψ_J yields

$$\sum_{L=0}^{N_{PC}} \sum_{J=0}^{N_{PC}} \hat{\boldsymbol{K}}_L \hat{\boldsymbol{u}}_J \left\langle \Psi_L \Psi_J \Psi_k \right\rangle = \sum_{L=0}^{N_{PC}} \left(\hat{\boldsymbol{F}}_L + \hat{\boldsymbol{Q}}_L \right) \left\langle \Psi_L \Psi_k \right\rangle \tag{18}$$

Solving (18) can obtain $\hat{u}_J \left(J = 0 \text{ to } N_{PC} \right)$. Accumulating the resulting $\hat{u}_J$ values can construct the generalized polynomial chaos expansion of u.

3. Results and Discussions

Two benchmark problems are introduced to evaluate the performance of (18) with adopting linear and high-order elements. The first benchmark problem involves a heat conduction problem over a square region. The second problem involves the transverse deflection of a square membrane.

3.1. Heat Conduction over a Square Region

As outlined by **Figure 1**, suppose a heat conduction problem over a unit square region in where ∇ is the gradient vector. The origin of x and y coordinates locates at the lower left corner. The boundaries $x = 0$ and $y = 0$ are insulated. The other boundaries $x = 1$ and $y = 1$ are maintained at zero temperature. In addition, the square region is subjected to a uniform heat generation.

To predict the temperature T, the governing equation is

$$-k \left(\frac{\partial^2 T}{\partial x^2} + \frac{\partial^2 T}{\partial y^2} \right) = q_0 \tag{19}$$

where k is the thermal conductivity and q_0 is the rate of uniform heat generation. In addition, the boundary conditions are

$$T\left(x = y = 1 \right) = \frac{\partial T\left(x = 0 \right)}{\partial y} = \frac{\partial T\left(y = 0 \right)}{\partial x} = 0 \tag{20}$$

Similarly manipulating (7), the deterministic finite element formulation of (19) is

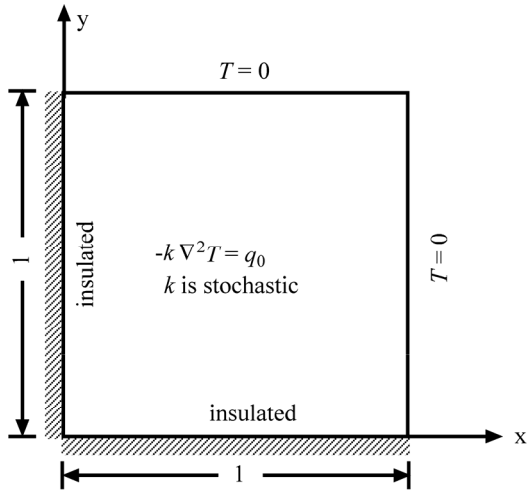

Figure 1. A heat conduction problem over a square region (not to scale).

$$\sum_{j=1}^{N} K_{ij}^e T_j^e = F_i^e \tag{21}$$

where

$$\begin{aligned} K_{ij}^e &= \int_{\Omega^e} k \left(\frac{\partial \psi_i}{\partial x} \frac{\partial \psi_j}{\partial x} + \frac{\partial \psi_i}{\partial y} \frac{\partial \psi_j}{\partial y} \right) \mathrm{d}x\mathrm{d}y \\ F_i^e &= \int_{\Omega^e} \psi_i^e q_0 \mathrm{d}\Omega \end{aligned} \tag{22}$$

Moreover, if the coefficient k is deterministic, the analytical solution of (19) is [8]

$$T = \frac{q_0}{2k} \left[1 - y^2 + 4 \sum_{n=1}^{\infty} \frac{\left(-1 \right)^n \cos\left(\alpha_n y \right) \cosh\left(\alpha_n x \right)}{\alpha_n^3 \cosh\left(\alpha_n \right)} \right] \tag{23}$$

where $a_n = \left(2n - 1 \right) \pi / 2$. However, the succeeding study considers that the thermal conductivity k is stochastic. Assume the distribution of k is described by

$$k = \mu_k \left[1 + \beta\left(x, y \right) \right] \tag{24}$$

where μ_k is the mean value of k and this μ_k value is independent upon x and y. Meanwhile, $\beta\left(x, y \right)$ is a zero-mean, scalar, homogeneous random field with its autocorrelation function Γ_β equal to

$$\Gamma_\beta = S_k^2 \exp\left[-\left(\frac{\left| x + \zeta_1 - x \right|}{d_1} + \frac{\left| y + \zeta_2 - y \right|}{d_2} \right) \right] \tag{25}$$

where d_1 and d_2 denote the correlation lengths, S_k is the standard deviation of thermal conductivity $k, \left(x + \zeta_1, y + \zeta_2 \right)$ and $\left(x, y \right)$ represent two points of the square region.

To compare the predicted temperature T with adopting linear or high-order elements, essential data is provided below

1) Define the problem domain Ω as $0 \le x \le 1$ and $0 \le y \le 1$.

2) Generate two cases of the finite element discretizations. As outlined by **Figure 2**, the left sub-figure denotes the first case which is composed of 25 nodes and 16 linear quadrilateral elements. The right sub-figure denotes the second case which is composed of 81 nodes and 16 quadratic (9-node) quadrilateral elements.

3) Consulting with **Table 1** and the previous study [6], experiment to represent k by the Lauguerre polynomial chaos. If the accuracy of corresponding spectral stochastic finite element results is unsatisfactory, apply another type of the generalized polynomial chaos.

4) Generate Monte Carlo simulation results to serve as the accuracy standard in evaluating the accuracy of spectral stochastic finite element results. A Monte Carlo simulation is implemented by first sampling the thermal conductivity k according to (24). Each sample of the thermal conductivity k is then substituted into (23) to predict a sample of the temperature T. If a sufficient amount of samples of k are created, the corresponding mean value μ_T and standard deviation S_T of temperature T will approach their exact values. These Monte Carlo simulation-based μ_T and S_T are computed by (e.g. [1])

$$\mu_T = \frac{1}{N_{\text{sample}}}\sum_{j=1}^{N_{\text{sample}}} T_j$$
$$S_T = \sqrt{\frac{1}{N_{\text{sample}}}\sum_{j=1}^{N_{\text{sample}}}\left[T_j - \mu_T\right]^2} \tag{26}$$

where N_{sample} is the total number of samples for implementing the Monte Carlo simulation, and the subscript j denotes T predicted using the j-th sample of thermal conductivity k. Meanwhile, similarly manipulating (16), the generalized polynomial chaos expansion of temperature T is $\sum_{i=0}^{N_{PC}}\hat{T}_i\Psi_i$ and the corresponding spectral stochastic finite element-based predicted μ_T and S_T are computed by (e.g. [1])

$$\mu_T = \hat{T}_0 \text{ and } S_T = \sqrt{\sum_{j=1}^{N_{PC}}\left(\hat{T}_j^2\right)\left(\Psi_j^2\right)} \tag{27}$$

5) Unless otherwise stated, the following parameters are adopted: $N_{\text{sample}} = 10^6, N_q = 16, d_1 = d_2 = 1,$ $N_{PC} = 10\left(n = 2, P = 3\right)$, $\mu_k = 1, S_k/\mu_k = 0.12$ in which N_q is the total number of quadrature points in a finite element.

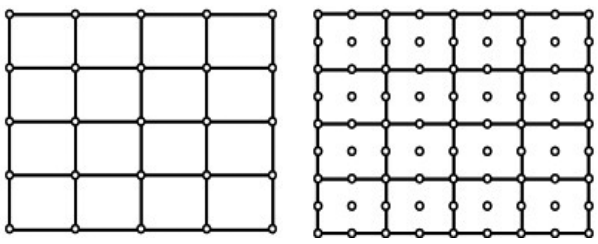

Figure 2. Finite element discretizations for analyzing the first benchmark problem (not to scale).

Furthermore, in an attempt of quantifying the errors between Monte Carlo simulation and spectral stochastic finite element results, two error estimators Δ_μ and Δ_S are defined below

$$\Delta_\mu(\%) = \frac{\left|\mu_{T,M} - \mu_{T,S}\right|}{\mu_{T,M}}, \Delta_S(\%) = \frac{\left|S_{T,M} - S_{T,S}\right|}{S_{T,M}} \tag{28}$$

in which the subscripts M and S denote the Monte Carlo simulation and spectral stochastic finite element method; respectively.

In (28), choosing $N_{\text{sample}} = 10^6$ is better checked by observing Monte Carlo simulation results with respect to different N_{sample} value. **Figures 3(a)** and **(b)** selectively checks variation of Monte Carlo simulation-based $\mu_T\left(x = y = 0\right)/q_0$ and $S_T\left(x = y = 0\right)/q_0$ versus different N_{sample} values.

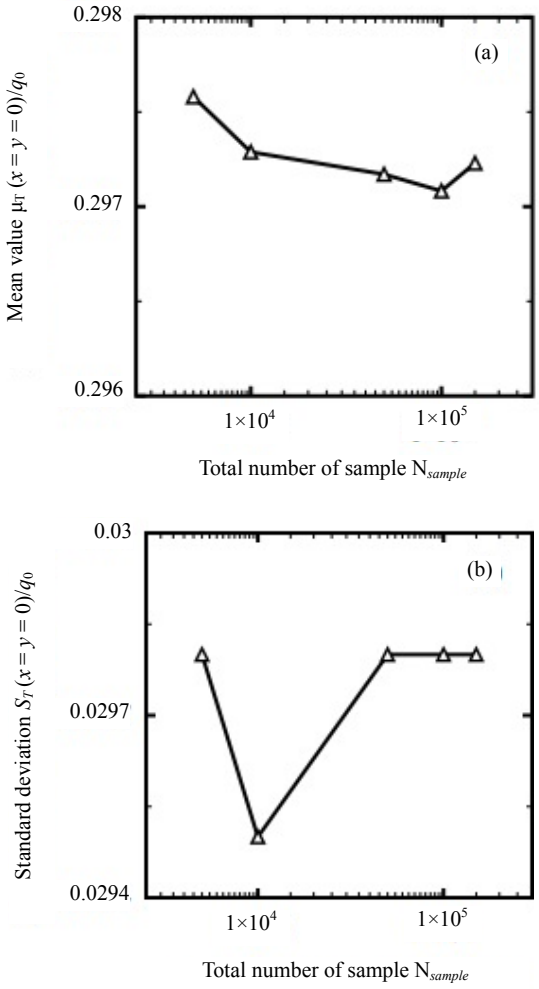

Figure 3. Variation of Monte Carlo simulation results with respect to different N_{sample} values: (a) mean value; (b) standard deviation (First benchmark problem).

Although the resulting $\mu_T(x=y=0)/q_0$ and $S_T(x=y=0)/q_0$ values range limitedly, **Figures 3(a)** and **3(b)** suggest that choosing $N_{\text{sample}}=10^6$ to implement a Monte Carlo simulation is reasonable. When more than 5×10^5 samples are created, the $\mu_T(x=y=0)/q_0$ and $S_T(x=y=0)/q_0$ values become stable.

Figures 4(a) and **(b)** selectively compare variation of $\Delta_\mu(y=0)/q_0$ and $\Delta_S(y=0)/q_0$ values with respect to **Figure 2**. In addition, **Table 2** compares the time spent to generate spectral stochastic finite element results with adopting linear and quadratic (9-node) quadrilateral elements. Note that all essential parameters, which are not listed in **Figures 4(a)** and **(b)** and **Table 2**, are set according to (28). Similar practices are followed in the following.

Since we can easily expect that adopting quadratic (9-node) elements can obtain more accurate deterministic finite element results, **Figure 4(a)** is not surprising. Adopting quadratic quadrilateral elements consequently predict more accurate mean values μ_T, since the corresponding $\Delta_\mu(y=0)/q_0$ is smaller. Nevertheless, **Figure 4(b)** is surprising. Adopting quadratic (9-node) elements can also obtain more accurate predicted standard deviation S_T values, since the corresponding $\Delta_S(y=0)/q_0$ values are smaller. Meanwhile, **Table 2** indicates that the time spent to generate spectral stochastic finite element results is not unacceptably time-consuming.

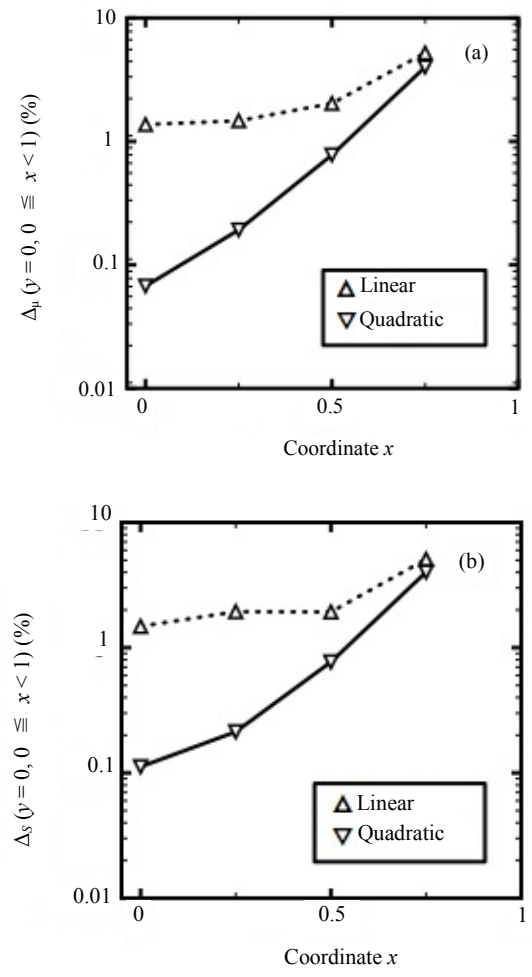

Figure 4. Comparison of accuracy of spectral stochastic finite element results with respect to linear and quadratic quadrilateral elements: (a) mean value; (b) standard deviation (First benchmark problem, μ = mean value, S = standard deviation).

Table 2. Comparison of the time spent to generate spectral stochastic finite element results adopting linear and quadratic (9 nodes) quadrilaterals.

Linear Elements	Quadratic Elements
1.2 seconds	1.5 seconds

*On a MacBook Pro with an Intel Core i5 Processor.

However, we may argue that **Figures 4(a)** and **(b)** only outline the effects of spacings of any two connecting nodes on the accuracy of spectral stochastic finite elements. As the nodal distribution becomes denser, obtaining more accurate spectral stochastic finite element results may be expected. To figure out this argument, the problem domain Ω is re-discretized by using 64 (8×8) linear quadrilateral elements and 81 equally-spaced nodes. Based on the resulting finite element discretization and **Figure 2(b)**, **Table 3** inspects variation of $\Delta_\mu(y=0)/q_0$ and $\Delta_S(y=0)/q_0$ values with respect to these two cases of finite element discretization.

Inspecting **Table 3** finds that adopting quadratic (9-node) elements still produces smaller $\Delta_\mu(y=0)/q_0$ and $\Delta_S(y=0)/q_0$ values. That is, the improvement of accuracy of spectral stochastic finite element results in **Figure 4(b)** is not due to the denser nodal distribution in the right sub-figure of **Figure 2**. In fact, comparing **Table 3** and **Figures 4(a)** and **(b)** finds that adopting a denser nodal distribution but still using linear elements only slightly improve the accuracy of spectral stochastic finite element results.

Furthermore, increase the S_k/μ_k value from 0.12 to 0.32. **Figures 5(a)** and **(b)** present the corresponding $\Delta_S(y=0)/q_0$ and $\Delta_S(y=0)/q_0$ values with respect to **Figure 2**. Next, change the d_2 value from 1.0 to 2.0 (but revert the S_k/μ_k value to 0.12). **Figures 6(a)** and **(b)** present the corresponding $\Delta_S(y=0)/q_0$ and $\Delta_S(y=0)/q_0$ values with respect to **Figure 2**.

The incentive of plotting **Figures 5(a)** and **(b)** comes from the published study [6] that high autocorrelation function values of stochastic coefficients (*i.e.* Γ_β values) has apparent effects on the accuracy of spectral stochastic finite element results. Further inspection of **Figures 5(a)** and **(b)** finds that adopting linear quadrilateral elements to apply the spectral stochastic finite element method

Table 3. Comparison of the time spent to generate spectral stochastic finite element results adopting linear and quadratic (9 nodes) quadrilaterals.

x	y	81 nodes and 64 linear quadrilaterals		81 nodes and 16 quadratic quadrilaterals	
		$\Delta_\mu(y=0)$	$\Delta_S(y=0)$	$\Delta_\mu(y=0)$	$\Delta_S(y=0)$
0.0	0.00	0.427	0.653	0.067	0.112
0.0	0.25	0.522	0.656	1.190	0.213
0.0	0.50	1.080	1.131	0.777	0.769
0.0	0.75	4.315	4.477	4.000	4.010

*Unit: $\Delta_\mu(y=0)$ and $\Delta_s(y=0)$ in %.

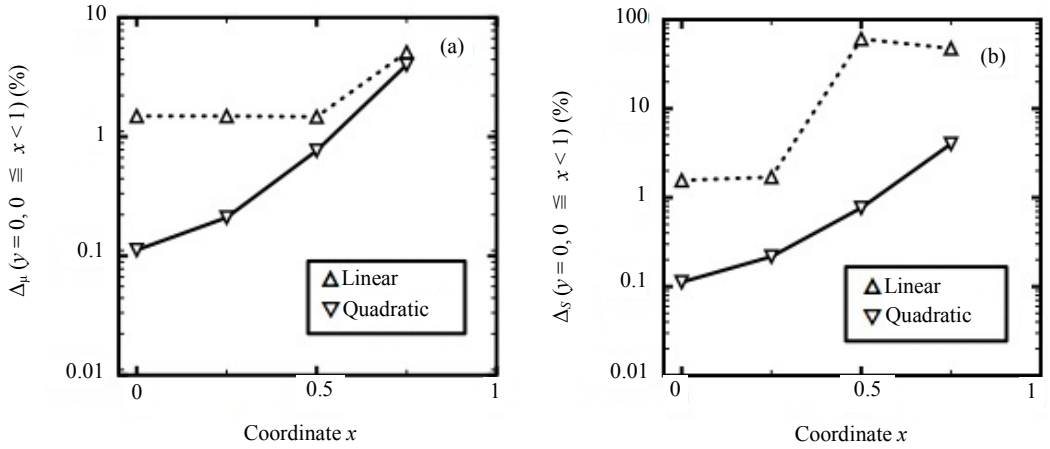

Figure 5. Comparison of accuracy of spectral stochastic finite element results with respect to $S_k/\mu_k = 0.32$, linear and quadratic quadrilateral elements: (a) mean value; (b) standard deviation (First benchmark problem, μ = mean value, S = standard deviation).

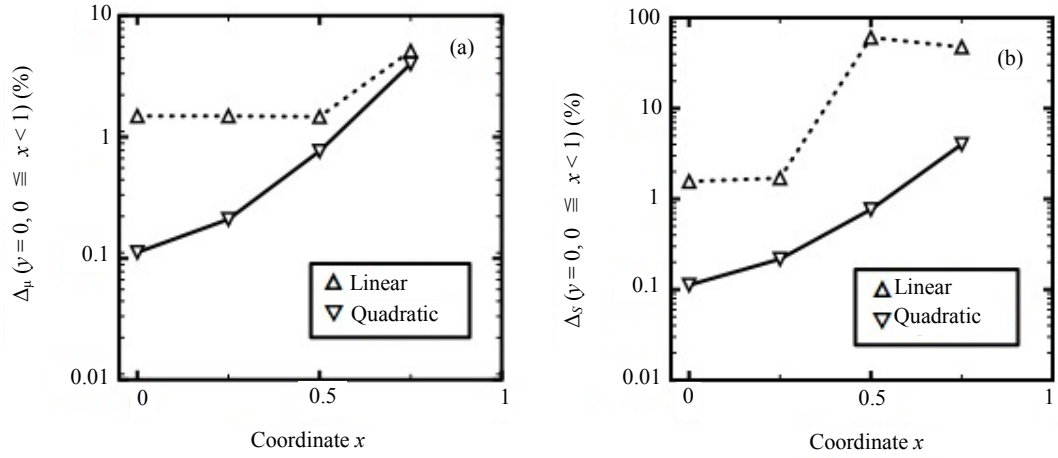

Figure 6. Comparison of accuracy of spectral stochastic finite element results with respect to d_2 = 2.0, linear and quadratic quadrilateral elements: (a) mean value; (b) standard deviation (First benchmark problem, μ = mean value, S = standard deviation).

may have the danger of obtaining uncontrollable $\Delta_S(y=0)/q_0$ values under high Γ_β values. **Figure 5(b)** denotes an example. If linear quadrilateral elements are adopted, some $\Delta_S(y=0)/q_0$ values approach 100%. Whereas, the $\Delta_S(y=0)/q_0$ values stay below 10% when quadratic (9-node) quadrilateral elements are used.

Meanwhile, **Figures 6(a)** and **(b)** indicate that the effects of different d_2 values on the $\Delta_\mu(y=0)/q_0$ and $\Delta_S(y=0)/q_0$ values are not noticeable. Comparing **Figures 4(a)** and **(b)** and **6(a)** and **(b)** finds that increasing d_2 values doesn't change the $\Delta_\mu(y=0)/q_0$ and $\Delta_S(y=0)/q_0$ values apparently.

3.2. Transverse Deflection of a Square Membrane

Suppose a membrane occupies a region $-2 \le x \le 2$ and $-2 \le y \le 2$ and its edges are fixed. Initially, the membrane is stretched so that the tension a in the membrane is uniform and that tension a is so large that it is not appreciably altered when the membrane is deflected by a distributed normal force f_0.

To predict the transverse deflection u of the membrane, the governing equation is

$$-a\left(\frac{\partial^2 u}{\partial x^2}+\frac{\partial^2 u}{\partial y^2}\right)=f_0 \tag{29}$$

Due to symmetry, only one quadrant of the membrane is analyzed. The boundary conditions are

$$\begin{aligned} u(x=y=1) &= \frac{\partial u(x=0)}{\partial y} \\ &= \frac{\partial u(y=0)}{\partial x}=0 \end{aligned} \tag{30}$$

Figure 7 further illustrates the layout of problem domain Ω and boundary conditions. If the tension a is deterministic, the analytical solution of u is

$$\frac{f_0}{2a}\left[\left(1-y^2\right)+4\sum_{n=1}^{\infty}\frac{(-1)^n\cos(\alpha_n y)\cosh(\alpha_n x)}{\alpha_n^3\cosh(\alpha_n)}\right].$$

Meanwhile, the deterministic finite element formulation of (30) is similar to (7) except that components K_{ij}^e and F_i^e are; respectively

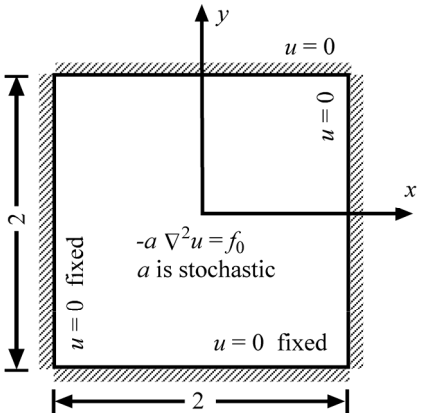

Figure 7. Transverse deflection of a square membrane (not to scale).

$$\int_{\Omega^e} a\left(\frac{\partial \psi_i}{\partial x}\frac{\partial \psi_j}{\partial x}+\frac{\partial \psi_i}{\partial y}\frac{\partial \psi_j}{\partial y}\right)\mathrm{d}x\mathrm{d}y \quad \text{and} \quad \int_{\Omega^e}\psi_i^e f_0 \mathrm{d}\Omega .$$

Nevertheless, the succeeding study assumes the tension a varies according to the following uniform distribution:

$$a=\mu_a+S_a^2\left(\zeta_3+\zeta_4\right) \tag{31}$$

where μ_a and S_a are; respectively, the mean value and standard deviation of tension a, $-1<\zeta_3,\zeta_4<1$ are two random numbers.

To compare the predicted deflection u with accounting for a stochastic tension a, essential data is provided below

1) Still define Ω as $0 \le x \le 1$ and $0 \le y \le 1$.

2) Generate two cases of the finite element discretizations. As outlined by **Figure 8**, the left sub-figure denotes the first case which is composed of 81 nodes and 64 linear quadrilateral elements. The right sub-figure denotes the second case which is composed of. 65 nodes and 16 quadratic (8-node) quadrilateral elements.

3) Consulting with **Table 1**, represent a by the Legendre polynomial chaos.

4) Generate Monte Carlo simulation results by first sampling the tension a according to (31). Each sample of the tension a is then substituted into the aforementioned analytical solution of (29) to predict a sample of the deflection u. Similarly manipulating (26), the mean value μ_u and standard deviation S_u of deflection u are equal to

$$\frac{1}{N_{\text{sample}}}\sum_{j=1}^{N_{\text{sample}}}u_j \quad \text{and} \quad \sqrt{\frac{1}{N_{\text{sample}}}\sum_{j=1}^{N_{\text{sample}}}\left[u_j-\mu_u\right]^2};$$

respectively. Meanwhile, the spectral stochastic finite element-based predicted μ_u and S_u are equal to $\hat{u}_0$ and $\sqrt{\sum_{j=1}^{N_{PC}}\left(\hat{u}_j^2\right)\left(\Psi_j^2\right)}$; respectively in which $\hat{u}_j$ ($j=0$ to N_{PC}) is obtained from the generalized polynomial chaos expansion of u.

5) Unless otherwise stated, the following parameters are adopted: $N_{\text{sample}}=10^6$, $N_q=16$, $N_{PC}=10\,(n=2,P=3)$, $\mu_a=1.0, S_a/\mu_a=0.1$.

Similarly manipulating Section 3.1, variation of the Monte Carlo simulation results versus different N_{sample} values and the accuracy of spectral stochastic finite ele-

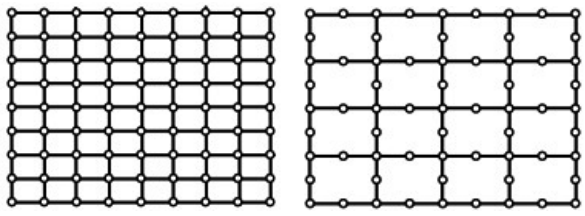

Figure 8. Finite element discretizations for analyzing the second benchmark problem (not to scale).

ment results are evaluated as follows: **Figures 9(a)** and **(b)** evaluate variation of Monte Carlo simulation-based predicted $\mu_u(x=y=0)$ and $S_u(x=y=0)$ with respect to different N_{sample} values. **Figures 10(a)** and **(b)** present variation of

$$\Delta_\mu(y=0, 0\le x<1)\left(\left|\mu_{u,M}-\mu_{u,S}\right|/\mu_{u,M}\right)$$

and

$$\Delta_S(y=0, 0\le x<1)\left(\left|S_{u,M}-S_{u,S}\right|/S_{u,M}\right)$$

values with respect to **Figure 8**. **Figures 11(a)** and **(b)** compare variation of $\Delta_\mu(y=0, 0\le x<1)$ and $\Delta_S(y=0, 0\le x<1)$ values with respect to **Figure 8** and $S_a/\mu_a=0.4$.

Figures 9(a) and **(b)** report that choosing $N_{\text{sample}}=10^6$ is still reasonable. As the N_{sample} value is larger than 10^6, the Monte Carlo simulation-based predicted $\mu_u(x=y=0)$ and $S_u(x=y=0)$ remain approximately fixed. Meanwhile, we still find from **Figures 10(a)** and **(b)** that adopting quadratic (8-node) elements is conducive to improving the accuracy of spectral stochastic finite elment-based predicted $S_u(y=0, 0\le x<1)$, since the corresponding $\Delta_S(y=0, 0\le x<1)$ value is smaller. Note that the total number of nodes in the left sub-figure of **Figure 8** is more than the total number of nodes in the right sub-figure of the same figure. Since similar results are found in **Table 3** and **Figures 4(a)** and **(b)**, adopting more nodes but still using the same element type consequently improve the accuracy of corresponding spectral stochastic finite element results slightly.

On the other hand, comparing **Figures 10(a)** and **(b)** with **Figures 11(a)** and **(b)** finds that

$$\Delta_\mu(y=0, 0\le x<1) \text{ and } \Delta_S(y=0, 0\le x<1)$$

values further increases versus the increase of S_a/μ_a values and the left sub-figure of **Figure 8**. However, the $\Delta_S(y=0, 0\le x<1)$ value in **Figure 11(b)** doesn't approach 100 %. This experience implies that different probability distributions of stochastic coefficients can produce different patterns of spectral stochastic finite element-based predicted mean values and standard deviations. Hence, the current study suggests doing some pilot tests to observe the performance of spectral stochastic finite element method versus a specific probability distribution of stochastic coefficients before practically applying this probability distribution.

4. Closure

As introduced in Section 1, the most popular numerical tool for solving stochastic partial differential equations may be the spectral stochastic finite element method. Numerous resources are available for generating spectral stochastic finite element results. As compared to the Monte Carlo simulation, applying the spectral stochastic finite element method doesn't require sampling the existing random fields sufficiently; thus, creating spectral stochastic finite element results is usually time-saving.

Probably since deterministic analytical solutions are usually unavailable for producing Monte Carlo simulation results, the accuracy of spectral stochastic is not often discussed and linear elements were usually adopted in applying this stochastic numerical method. However, the succeeding study demonstrates that adopting high-order (e.g. quadratic) elements can improve the performance of spectral stochastic finite element method. The previous section has shown that adopting linear elements has the danger of obtaining uncontrollable errors between Monte Carlo simulation and spectral stochastic finite element results. Whereas, adopting quadratic (9-node or 8-node) elements to apply the spectral stochastic finite element method stably produces more accurate predicted

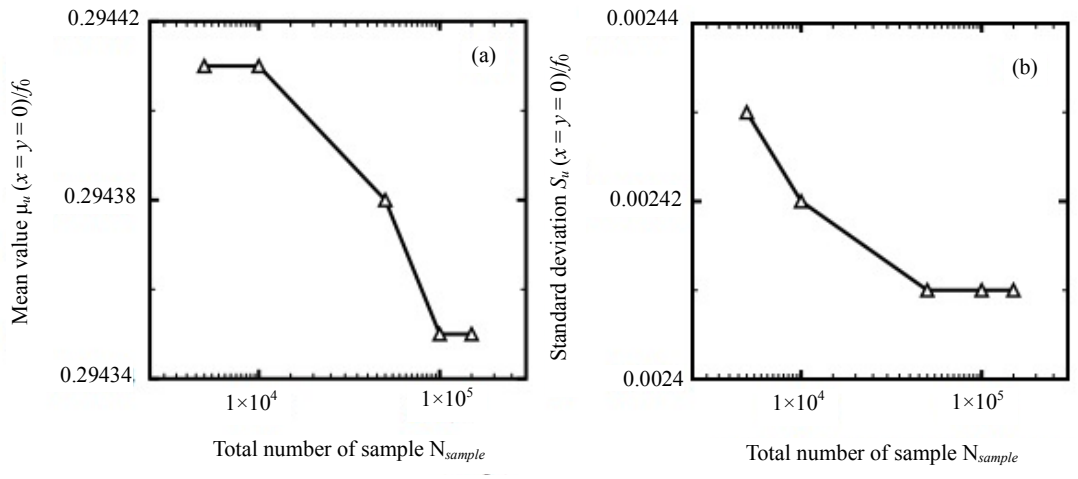

Figure 9. Variation of Monte Carlo simulation results with respect to different N_{sample} values: (a) mean value; (b) standard deviation (Second benchmark problem).

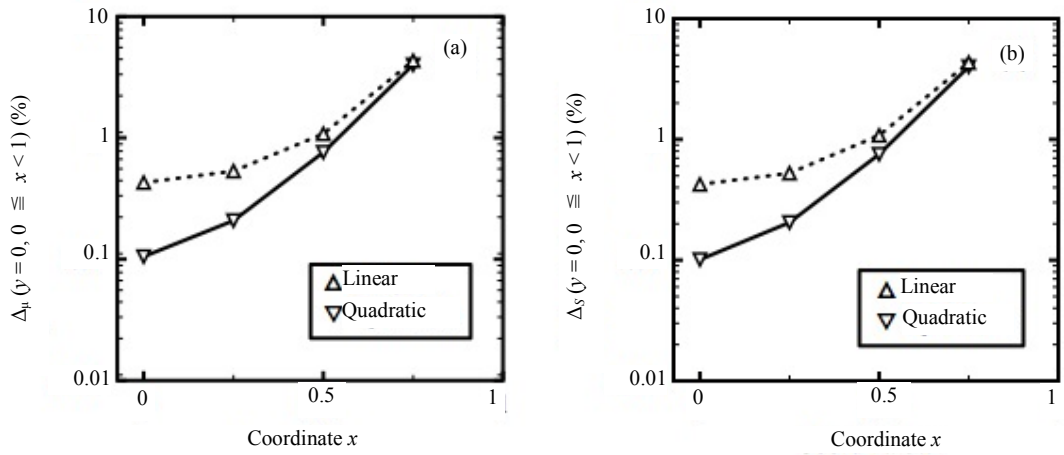

Figure 10. Comparison of accuracy of spectral stochastic finite element results with respect to linear and quadratic quadrilateral elements: (a) mean value; (b) standard deviation (Second benchmark problem, μ = mean value, S = standard deviation).

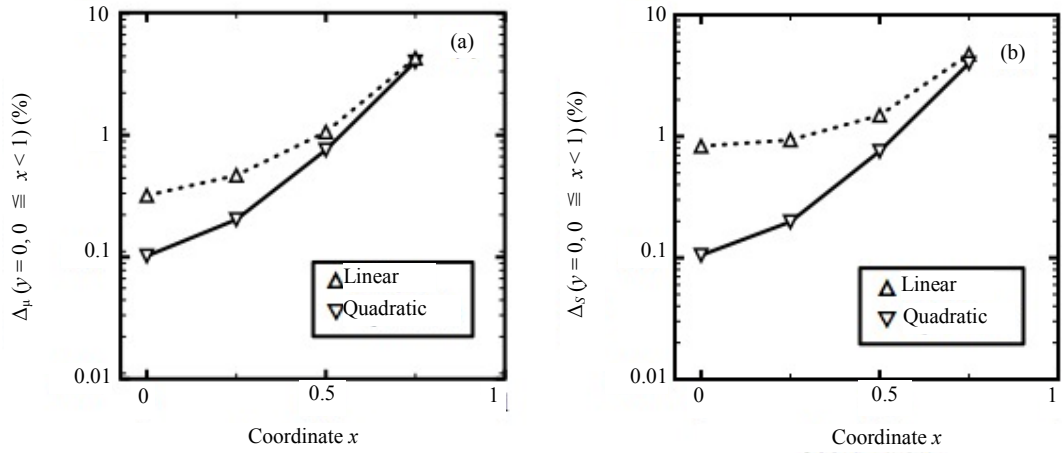

Figure 11. Comparison of accuracy of spectral stochastic finite element results with respect to $S_k/\mu_k = 0.4$, linear and quadratic quadrilateral elements: (a) mean value; (b) standard deviation (Second benchmark problem, μ = mean value, S = standard deviation).

mean values and standard deviations under high autocorrelation function values of existing stochastic coefficients ranges. In addition, the time spent to apply the spectral stochastic finite element method with using quadratic quadrilateral elements is not unacceptably time-consuming.

In conclusion, replacing linear elements with high-order elements to apply the spectral stochastic finite element method can be as a low-cost method to improve the performance of this stochastic numerical method.

REFERENCES

[1] R. G. Ghanem and P. D. Spanos, "Stochastic Finite Elements: A Spectral Approach," Springer-Verlag, New York, 2012.

[2] D. Xiu and G. E. Karniadakis, "Modeling Uncertainty in Flow Simulations via Generalized Polynomial Chaos," *Journal of Computational Physics*, Vol. 187, No. 1, 2003, pp. 137-167. doi:10.1016/S0021-9991(03)00092-5

[3] M. Loève, "Probability Theory II (Graduate Text in Mathematics)," Springer-Verlag, Berlin, 1978.

[4] S. Q. Wu and S. S. Law, "Evaluating the Response Statistics of an Uncertain Bridge-vehicle System," *Mechanical Systems and Signal Processing*, Vol. 27, 2012, pp. 576-589. doi:10.1016/j.ymssp.2011.07.019

[5] V. Papadopoulos and O. Kokkinos, "Variability Response Functions for Stochastic Systems," *Probabilistic Engineering Mechanics*, Vol. 28, 2012, pp. 176-184. doi:10.1016/j.probengmech.2011.08.002

[6] G. Y. Sheu, "Prediction of Probabilistic Settlements via Spectral Stochastic Meshless Local Petrov-Galerkin Method," *Computers and Geotechnics*, Vol. 38, No. 4, 2011, pp. 407-415. doi:10.1016/j.compgeo.2011.02.001

[7] M. F. Ngah and A. Young "Application of the Spectral Stochastic Finite Element Method for Performance Pre-

diction of Composite Structures," *Composite Structures*, Vol. 78, No. 3, 2007, pp. 447-456. doi:10.1016/j.compstruct.2005.11.009

[8] J. N. Reddy, "An Introduction to the Finite Element Method," 2nd Edition, McGraw-Hill Company, New York, 1993.

